Study of CC2p0π Event Topologies in the MicroBooNE Detector

MICRBOONE-NOTE-1096-PUB

The MicroBooNE Collaboration*

August 30th, 2021

Abstract

The precise measurement of neutrino oscillation parameters is a critical component of understanding neutrino oscillations. As future accelerator neutrino experiments will utilize ^{40}Ar as the target nucleus it is important to understand the influence that nuclear effects have on neutrino-nucleon cross-sections. Processes that lead to 2 particle-2 hole (2p2h) states are of particular interest, such as Meson Exchange Currents (MEC) and Short Range Nucleon-Nucleon Correlations. In the MicroBooNE detector, a charged-current interaction that produced a 2p2h state would create a 3 track topology with 1 muon and 2 protons connected to a single interaction vertex (CC2p0π). We present here a study of MicroBooNE's potential sensitivity to a variety of MEC models as well as CC2p0π events selected from a combination of data collected from the first 3 years of running of the MicroBooNE experiment.

*Email: MICROBOONE_INFO@fnal.gov

Contents

1 Introduction & Motivation

In addition to its investigation of the MiniBooNE Low-Energy Excess [1], MicroBooNE supports a variety of cross-section analyses, since the precise understanding of neutrino cross-sections on ^{40}Ar is critical to the success of future oscillation experiments. One topic of interest is the characterization of 2-particle 2-hole states (2p2h): events in which 2 particles are removed from the nucleus leaving it in a 2 hole state. Two processes that can lead to 2p2h states are Short-Range Nucleon-Nucleon Correlations (SRC), in which the leptonic probe interacts with a single nucleon in a correlated pair and ejects both nucleons, and Meson Exchange Currents (MEC), in which the momentum transfer is shared between two uncorrelated nucleons. While both of these processes contribute non-trivially to neutrino cross-sections, there is no generally accepted way to model their contributions. Further, many neutrino interaction models do not take into account the contribution of SRCs to the cross-section at all.

A first measurement of CC2p0π events in ^{40}Ar was conducted by the ArgoNeuT collaboration. The study, even if statistically limited, suggested that mechanisms involving nucleon-nucleon SRC are active [2]. This analysis aims to utilize a variety of different theoretical models as well as MicroBooNE's large dataset to study MECs and eventually SRCs. Section 2 will introduce the different MEC theoretical models to be studied by this analysis as well as provide some initial model comparisons. This section will also introduce some variables that are sensitive to differences between these models. Section 3 will introduce the MicroBooNE detector. Section 4 will introduce the various data samples used by this analysis. Section 5 will provide the signal definition and detail the event reconstruction and selection. Section 6 will show initial event distributions of events selected from MicroBooNE data. Section 7 will describe our future plans for the analysis.

2 Theoretical Discussion

In the MicroBooNE detector, a charged-current interaction that produced a 2p2h state would create a 3 track topology with 1 muon and 2 protons connected to a single interaction vertex. While this event topology can also be produced by Resonant Pion Production (RES) and Final State Interactions (FSI), this analysis will focus primarily on contributions from MECs. In this analysis, a study was conducted to identify variables that showed sensitivity to differences found in events generated from three different MEC model sets. More details on MECs and the theoretical study can be found below.

2.1 Meson Exchange Currents

Meson exchange currents occur when the momentum transfer is shared between two nucleons via the exchange of a virtual meson between the two nucleons, causing both to be ejected from the nucleus. In electron scattering experiments, it was observed that the differential cross-section as a function of energy transfer exhibited a deeper dip than expected in between the quasi-elastic (QE) and Δ-resonance peaks. With the addition of contributions from MECs, some models were able to account for the increased depth of the dip with data from electron scattering experiments. Cross-section results from the MiniBooNE collaboration were also successfully produced by some groups with the addition of effects from MECs [3]. While it is clear that the addition of MECs is crucial to understanding both electron and neutrino scattering data, there is no single generally accepted model. In our analysis, we consider events generated from 3 model sets found within GENIE, each with differing MEC models. These model sets are listed below, along with the GENIE tune strings [4]. Each set of models also uses the hA2018 FSI model is to be consistent with the MicroBooNE GENIE Tune.

- G18_02a_00_000 : Empirical MEC + Lwellyn-Smith QE [3]
- G18_10a_02_11a: Nieves/Valencia Model (QE + MEC) [5]
- G21_11b_00_000: SuSAv2 (QE + MEC) + hA2018 FSI [6]

2.2 Initial Model Comparisons

In order to make initial comparisons between the three different model sets, two cuts were applied to select generated events with kinematic limits consistent with the MicroBooNE detection efficiency for muons and protons. Selected events have 1 muon with momentum between 0.1 and 1.2 GeV/c, and two protons with momentum between 0.3 and 1.0 GeV/c. The proton with the most momentum is labeled as the leading proton (P_L) and the other proton is labeled as the recoil proton (P_R) The number of events remaining after these 2 cuts in each sample can be found in Table 1.

Cut	Empirical	Nieves	SuSAv2
Initial	4000000 (100%)	2400000 (100%)	3800000 (100%)
$0.1 < P\mu < 1.2$ GeV/c	3523603 (88.1%)	216638 (88.2%)	3350683 (88.2%)
$0.3 < P_{L,R} < 1.0$ GeV/c	542167 (13.6%)	295622 (12.3%)	598444 (15.7%)

Table 1: Number of events remaining after each cut in the Empirical, Nieves, and SuSAv2 samples.

To understand the impact that these models have on event distributions, events selected from the four samples were plotted as a function of a variety of variables expected to be sensitive to the differences. The distributions were then area normalized to allow for shape differences to be studied between the different models. Distributions from all the variables studied can be found in Appendix A.1. Three variables were identified.

The first variable that shows sensitivity to the differences between the models is the momentum of the three different particles, found in Figure 1. We see a difference in the location of the peak between the Empirical model compared to the other two models in the muon momentum (top). Furthermore, we see slight shape differences between all three models in the leading proton momentum (bottom left). All three models have similar predictions for the recoil proton momentum (bottom right).

The second variable that shows differences between the different MEC models is the opening angle between the two protons measured in the lab frame (denoted γ_{Lab}). The cosine γ_{Lab} can be found in 2. The Empirical model set exhbits an additional bump around $\cos(\gamma_{\text{Lab}}) \approx$ -0.3 compared with the other models. Furthermore, the Nieves model set predicts more events at $\cos(\gamma_{\text{Lab}}) = 1$ than the other models, but the SuSAv2 model set predicts more events at $\cos(\gamma_{\text{Lab}}) =$ -1.

The final variable that exhibits sensitivity to differences between the different MEC models is the opening angle between the muon momentum and the total proton momentum vector (denoted $\gamma_{\mu,\text{p}_{\text{Lead}}+\text{p}_{\text{Recoil}}}$). The cosine of $\gamma_{\mu\text{p}_{\text{Lead}}+,\text{p}_{\text{Recoil}}}$ can be found in Figure 3.

The variables identified above provide insight into the effect that the differences between these models have on these distributions.Events selected from these model sets must be compared to events selected from real data in order to determine which differences are actually observable. The samples used and the process of developing an event selection in data will be described in the following sections.

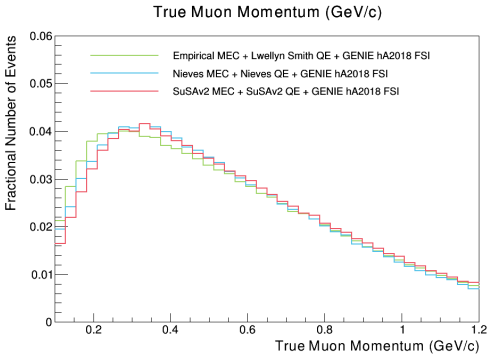

(a) Muon momentum.

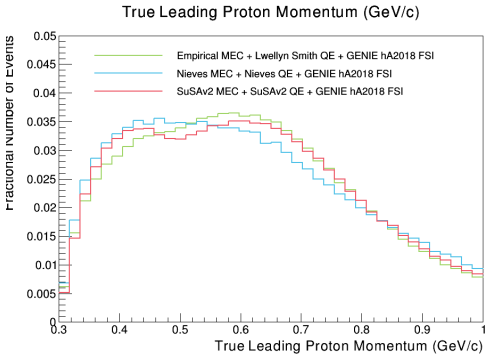

(b) Leading Proton momentum.

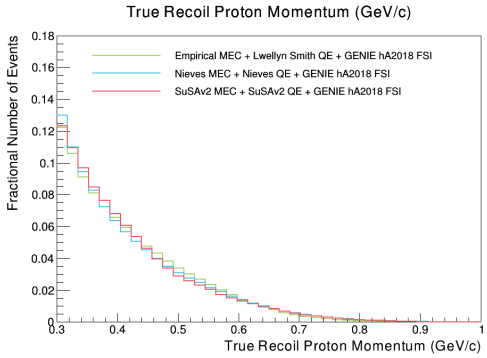

(c) Recoil Proton momentum.

Figure 1: Momentum of the three particles for the three different MEC model sets

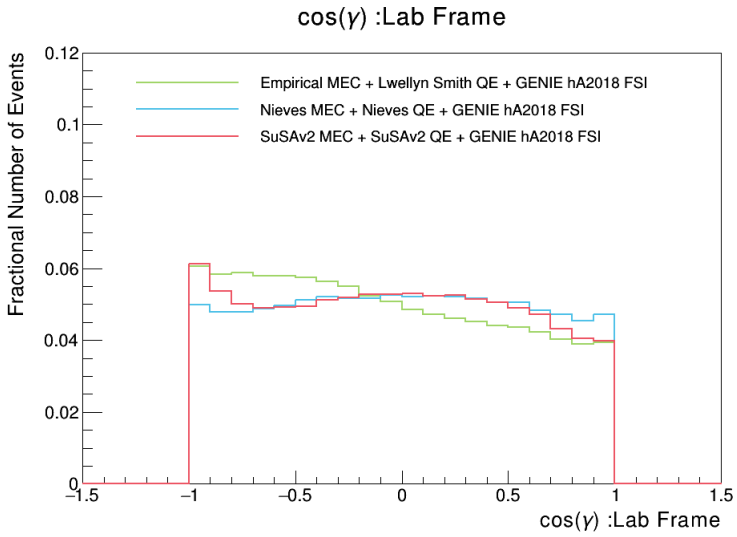

Figure 2: $\cos(\gamma_{\text{Lab}})$ for the three different MEC model sets.

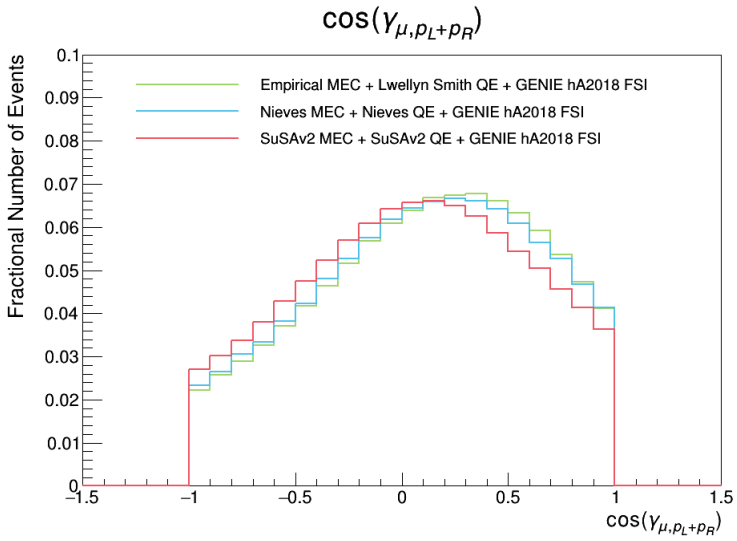

Figure 3: $\cos(\gamma_{\mu,\mathrm{p_{Lead}}+\mathrm{p_{Recoil}}})$ for the three different MEC model sets.

3 The MicroBooNE Experiment

MicroBooNE is a liquid argon time projection chamber (LArTPC) located in the Booster Neutrino Beam (BNB) at Fermi National Accelerator Laboratory. A cut open view of the detector can be seen in Figure 4. The detector consists of a cylindrical cryostat filled with 170 tons of liquid argon,, a photomultiplier tube (PMT) rack (mounted on the left hand side in the image), and a TPC (the cuboid located within the cryostat) that is 10.5 m long in the beam direction, 2.56 m wide in the drift direction, and 2.35 m tall (active mass of 85 tons) [7].

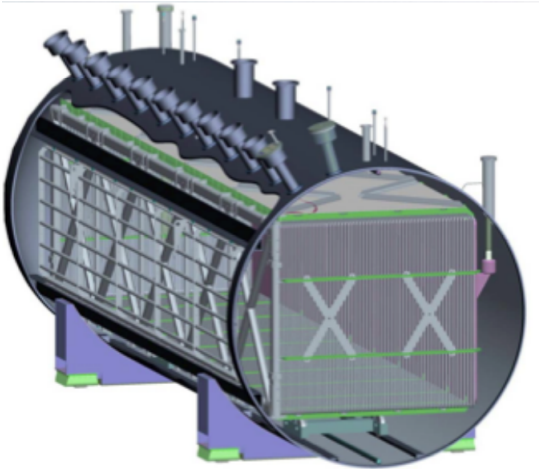

Figure 4: Cut open view of the MicroBooNE detector.

A diagram of how a neutrino event is detected can be seen in Figure 5 below. When neutrinos from the BNB (purple) interact with argon atoms (yellow) within the cryostat they produce charged particles (the muon and proton in this case). The interaction of the charged particles moving in the liquid argon produces an ionization trail, as well as scintillation light. The scintillation light that is produced from the interaction is collected by the 32 8-inch PMTs located behind the anode plane. This information will later be used in the reconstruction and rejection of cosmic rays. The electrons resulting from the ionization (pink) are directed through the detector by the 273 V/cm drift field produced by the cathode plane (grey). As the electrons drift through the detector, they are detected by 3 planes of wires: the collection plane with wires oriented vertically, known as the Y plane (yellow), and two induction planes with wires $\pm 60^\circ$ with respect to the Y plane, known as the U (blue) and V (green) planes. As the electrons pass by the U and then V induction planes, the induced signal is measured. These planes are also at a slight lower electric potential in order to prevent electrons from being collected onto them. After passing the induction planes, the electrons are then collected by the Y plane.

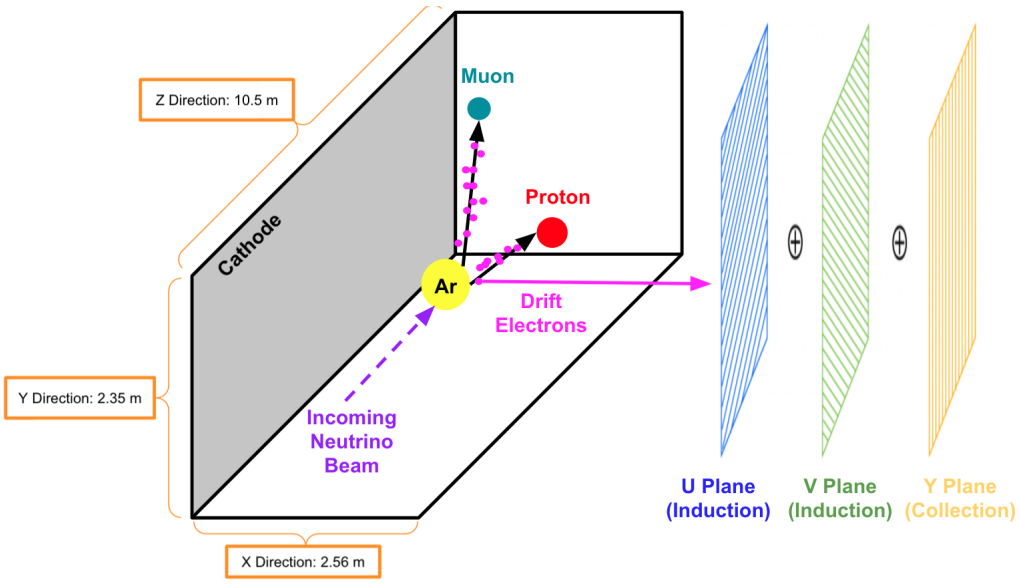

Figure 5: Sketch of a neutrino event and its detection within MicroBooNE.

By mapping the location and magnitude of the charge deposited on each wire plane as a function of the drift time, 2D images can be produced which replicate the full topology of the neutrino event. A sample of one of these images of a selected CC2p0π in BNB-data can be seen in Figure 6 below.

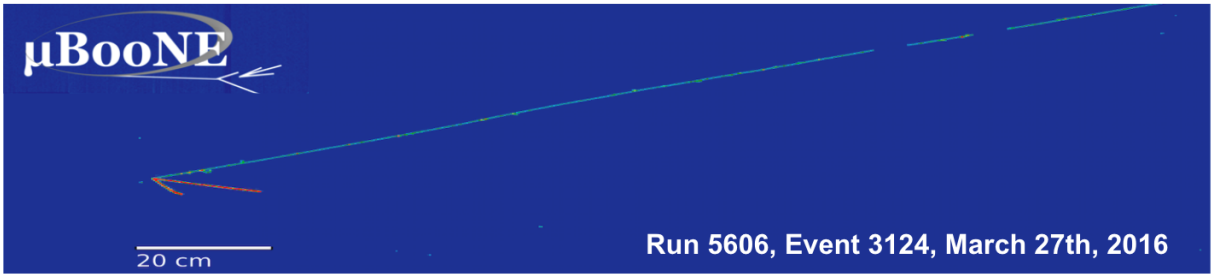

Figure 6: BNB Neutrino event recorded in MicroBooNE during Run 1 data taking. The x-axis is the wire number in the V plane and the y-axis is the drift time. The color represents the charge deposition. The two smaller red tracks are proton candidates (large charge deposition), and the long light blue track is a muon candidate (small charge deposition). This event was identified as a CC2p0π event by the selection described in this note.

In the above image, the x-axis is the wire number in a specific plane and the y-axis is the drift time. The color within the image represents the amount of measured charge detected by the wire planes, which is a measure of the energy deposited by the particles. In this scale, red means a large amount of charged was detected, and blue means a small amount of charge was detected. [8].

4 Samples

This analysis utilizes a data sample corresponding to 6.79×10^{20} protons-on-targe (POT) collected from the first 3 years of MicroBooNE's running. This on-beam data stream (BNB-data) is collected when scintillation light is detected in coincidence with a 1.6 μs BNB neutrino spill. In addition to on-beam data, off-beam data (EXT-data) is also collected. This stream is collected when no beam is present, with the same scintillation light requirements in a false beam window. Since MicroBooNE is a near surface detector with minimal shielding, this sample is critical in the characterization of MicroBooNE's cosmic ray background.

In addition to using our EXT data, MicroBooNE also employs cosmic-data-overlaid Monte-Carlo (MC) events to help develop analyses. This MC sample (MC-Overlay) utilizes cross-section models found in GENIE 3.0.6 as a base for the neutrino interaction modeling. A variety of corrections are then applied to these base models in order to create the MicroBooNE Tune. A more detailed explanation of this process can be found in [9]. The MicroBooNE Tune currently uses a tuned version of the Nieves/Valencia model to describe the QE and MEC processes. The MicroBooNE Tune also uses an untuned version of the hA2018 FSI model.

In addition to the MC-Overlay, MicroBooNE analyses also make use of MC generated events of neutrino interactions that occur outside of the TPC. This MC sample (MC-Dirt) is used to help analyses constrain backgrounds created by these events.

5 Event Reconstruction and 1μ2p Event Selection

5.1 Signal Definition

This analysis aims to select events with 1 muon and 2 protons in the final state. Events must fulfill the following requirements to be considered signal:

- A single muon with momentum greater than 100 MeV/c, but less than 1.2 GeV/c.
- Two protons with momentum greater than 300 MeV/c, but less than 1.0 GeV/c.
- No charged pions with momentum above 65 MeV/c.
- No neutral pions of any momentum.
- The simulated vertex must be within the defined fiducial volume (10 cm from any TPC face).

5.2 Event Reconstruction

After data is collected, events undergo signal processing to remove noise and convert the ADC waveforms into Gaussian-shaped signals [10, 11]. These 2D signals, known as hits, are then combined to form 3D objects known as Particle Flow Particles (PFPs) using the Pandora multi-algorithm pattern recognition framework [12, 13]. This conversion allows for PFPs to be classified as tracks or showers, and for their parent-child relationships to other PFPs to be determined. Pandora then employs a number of algorithms to cluster the PFPs into slices based on their relative location to one another in the detector. After the slices are identified, a tool - known as the NeutrinoID - uses optical and geometric information to reject obvious cosmic slices. The tool then uses a Support Vector Machine (SVM) to select the slice with the highest likelihood of being the neutrino slice [14].

5.3 Event Selection

In order to select 1μ2p events, data must first be filtered to select events containing 3 tracks (also known as three prong events). The following cuts are applied to select three prong events:

- The reconstructed neutrino vertex must lie within the fiducial volume (defined to be 10 cm from any TPC face).
- There must be exactly 3 PFPs with the following attributes:

– The PFP's track score must be above 0.8 [13].

– The PFP's track start must be within 4 cm of the reconstructed vertex.

A plot of the track score can be found in Figure 7, plotted immediately following the 3 PFP requirement. The track score is a variable designed to distinguish tracks from showers. In Pandora, the default track score value is set to 0.5 i.e. a PFP is shower-like if it has a track score below 0.5, and track-like it its track score is above 0.5. As seen in our plot of the track score, using a cut value of 0.8 allows us to keep a majority of the muon and proton tracks, the particles of interest to this analysis, but also cut out more background.

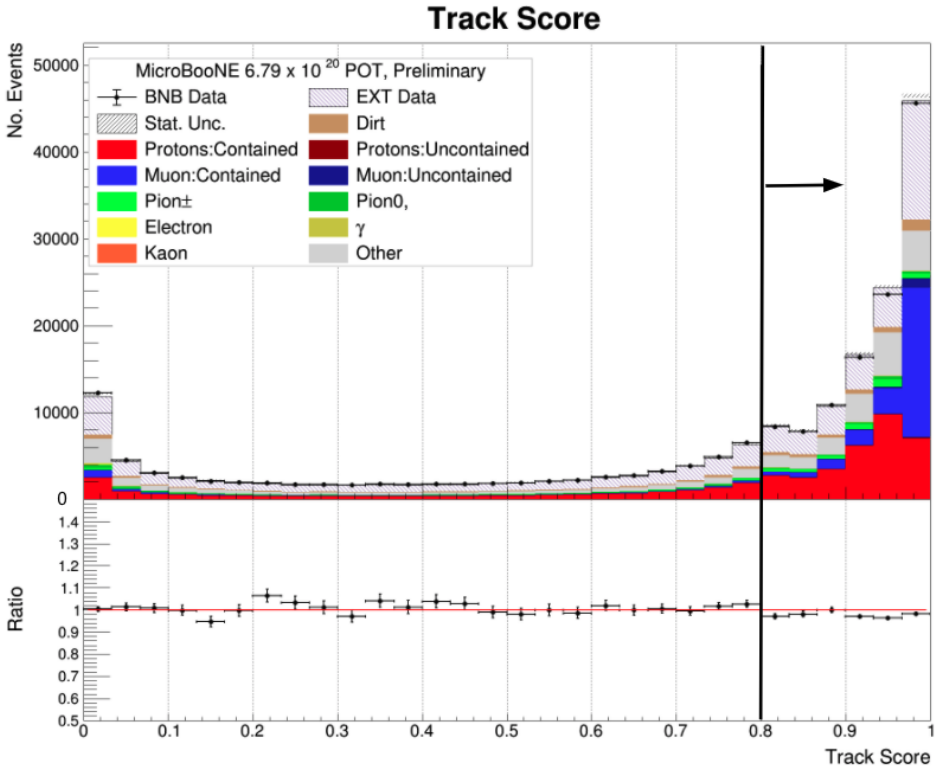

Figure 7: Track score for each track in the events with exactly 3 PFPs.

A plot of the track vertex distance can be found in Figure 8. This variable measures the 3D distance between the reconstructed start of the track to the location of the reconstructed vertex. We require that all 3 tracks are within 4 cm of the vertex (to the left of the line in Figure 8) in order to remove additional backgrounds that may be present in the neutrino slice.

Once three prong events are selected, Particle Identification (PID) can be utilized to select $1\mu 2p$ events. We utilize a quantity known as the Log-Likelihood Ratio (LLR) PID [15]. The method compares the measured dE/dx profile of a track with a probability density function (PDF) of dE/dx. The PDF of the dE/dx profile is unique to each track, and includes information from all 3 planes in order to account for distortions for tracks with a large local pitch and for angular dependencies in the calorimetric reconstruction. The resulting LLR value indicates whether a track is more muon-like (an LLR value of 1) or proton-like (an LLR value of -1). The distribution of the LLR for all tracks in events selected by our 3 prong selection can be found in Figure 9. As expected, the protons (in red) and the muons (in blue) fall into two distinct populations, with minor proton contamination seen in the muon population and minor muon contamination seen in the proton population. To be consistent with other analyses [16], we classify a track as a muon if it has an LLR PID score above 0.2, and classify a track as a proton if it has an LLR PID score below 0.2. We require that there is exactly 1 track identified as a muon, and 2 tracks identified as protons based on the previously mentioned condition. This selects our $1\mu 2p$ events.

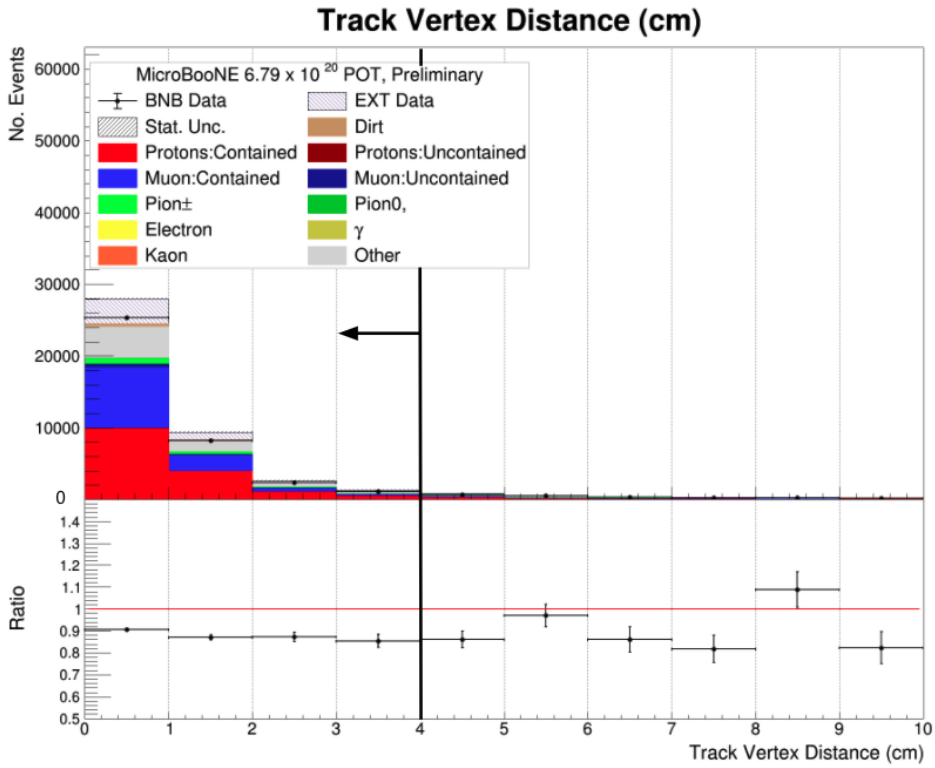

Figure 8: 3D distance from the track start to the reconstructed vertex for each track in events with exactly 3 PFPs and each PFP has a track score above 0.8.

5.4 Particle Momentum

In order to accurately reconstruct the momentum of all particles, we require that the identified muon and both protons are contained. A track is considered to be contained if the reconstructed start of the track is within the FV (10 cm from any TPC face) and the reconstructed end of the track is within the TPC. The requirement of containment allows for range-based momentum reconstruction techniques to be utilized. Once the momentum of all three particles is known, we can distinguish the two protons by labeling the proton with the most momentum as the leading proton, and the other proton as the recoil proton. In addition to the containment requirement, we reject events in which the muon, lead, or recoil proton momentum are located in phase-space regions of low efficiency. Specifically, the muon must have reconstructed momentum between 0.1 GeV/c and 1.2 GeV/c and the protons must have momentum between 0.3 GeV/c and 1.0 GeV/c. These limits are consistent with the kinematic limits of our signal definitions.

5.5 Efficiency and Purity of Applied Selection

The efficiency and purity of the selection can be defined as the following:

$$\text{Efficiency} = \frac{\text{Number of True } 1\mu 2\text{p Events That Pass All Cuts}}{\text{Number of True } 1\mu 2\text{p Events}} \tag{1}$$

$$\text{Purity} = \frac{\text{Number of True } 1\mu 2\text{p Events That Pass All Cuts}}{\text{Number of Events That Pass All Cuts}} \tag{2}$$

The efficiency and purity of the selection are 13% and 65.4% respectively.

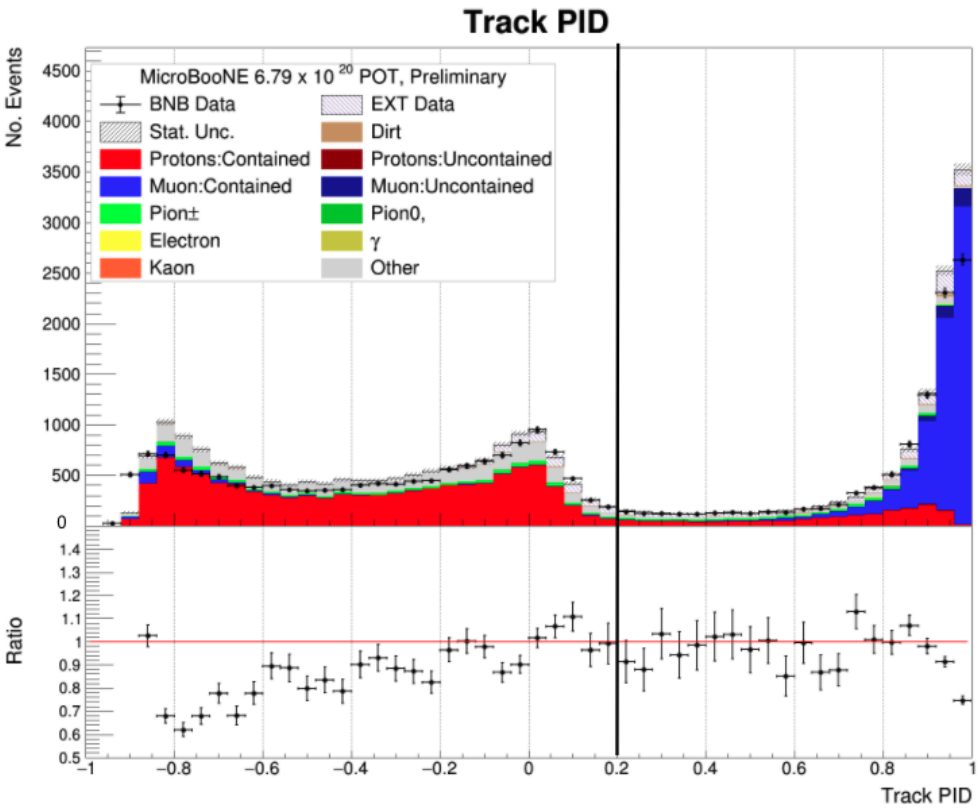

Figure 9: The Log-Likelihood Ratio for each track in the selected 3 prong events.

5.6 Selected Events

Table 2 shows the number of events selected from the 4 different samples. After all the cuts are applied, a majority of the background are eliminated, leaving less than 1% of the initial number of events in each sample. A total of 3157 events are selected in BNB-data, 186 are selected in EXT data, 13097 are selected in MC-Overlay, and 21 are selected in MC-Dirt.

	BNB Data	EXT Data	MC-Overlay	MC-Dirt
Initial	595683 (100%)	5218826 (100%)	2923785 (100%)	516737 (100 %)
Vertex in FV	328531 (55.2%)	351700(6.7%)	866009(29.6%)	33436 (6.47%)
Exactly 3 PFPs	67407 (11.3%)	60501 (1.16%)	200410 (6.85%)	4903 (0.95%)
3 Tracks with Score above 0.8	15231 (2.56%)	6741 (0.13%)	61328 (2.10%)	620 (0.12%)
3 Tracks within 4 cm of Vertex	8055 (1.35%)	1841 (0.04%)	33811 (1.16%)	131 (0.03%)
1 Track >0.2 2 Tracks <0.2	5642 (0.95%)	598 (0.01%)	22467 (0.77%)	50 (0.01%)
Containment Cut	4668 (0.80%)	361 (0.01%)	18078 (0.62%)	34 (0.01%)
Reco. Momentum Cut	3157 (0.53%)	186 (0.01%)	13097 (0.45%)	21 (0.01%)

Table 2: Number of events remaining after each cut in the BNB data, EXT data, MC-Overlay, and MC-Dirt samples.

The 13097 selected MC-Overlay events are also divided based on truth information into two different sets of MC definitions. Table 3 shows the distribution of MC events as a function of different final states.

As expected $1\mu 2p$ (highlighted in pink) constitutes the largest portion of selected events. Table 4 shows the distribution of MC-Overlay events as a function of neutrino interactions. $1\mu 2p$ events can be produced by a number of different interactions, include QE, MEC, and RES. These interactions constitute the largest portion of the selected events with CCRES being the largest at 32.3 % of selected MC-Overlay events.

	Number of Events	% of Total
Total Selected	13097	100%
CC0p0π	149	1.14%
CC1p0π	722	5.51%
CC2p0π	8566	65.4%
CC(N>2)p0π	909	6.94%
CC(N>=0)p1π	981	7.49%
CC(N>=0)p(N>1)π	31	0.24%
CCNue	4	0.03%
NC	659	5.03%
Out of FV	379	2.89%
Else	697	5.32%

Table 3: Table showing the distribution of 13097 selected overlay events in terms of different final state topologies. CC2p0π (our event signal), is highlighted in light pink.

	Number of Events	% of Total
Total Selected	13097	100%
CCQE	2999	22.9%
CCRES	4578	34.9%
CCMEC	4146	31.7%
CCDIS	332	2.53%
CCCOH	0	0.0%
CCNue	4	0.03%
NC	659	5.03%
Out of FV	379	2.89%

Table 4: Table showing the distribution of 13097 selected overlay events in terms of different neutrino interaction channels.

6 Event Distributions

The momentum (as calculated from range) of the muon (top), leading proton (middle), and the recoil proton (bottom) can be seen in Figure 10, where the selected Overlay MC events are divided into different topologies on the left, and different neutrino interaction channels on the right. Note that the BNB-data (black points) only contains statistical uncertainties at this time.

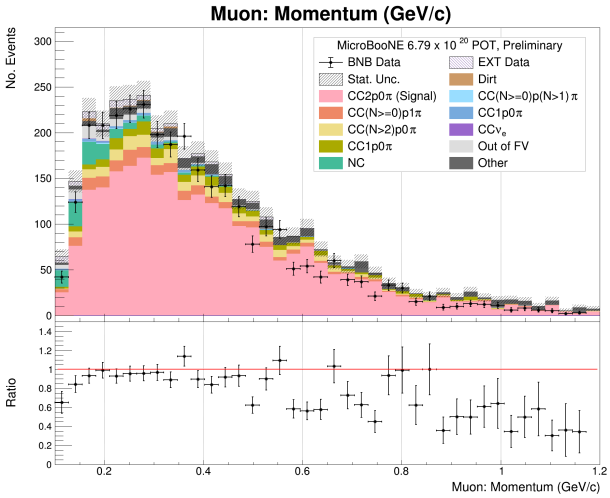

(a) Muon momentum: ν topologies.

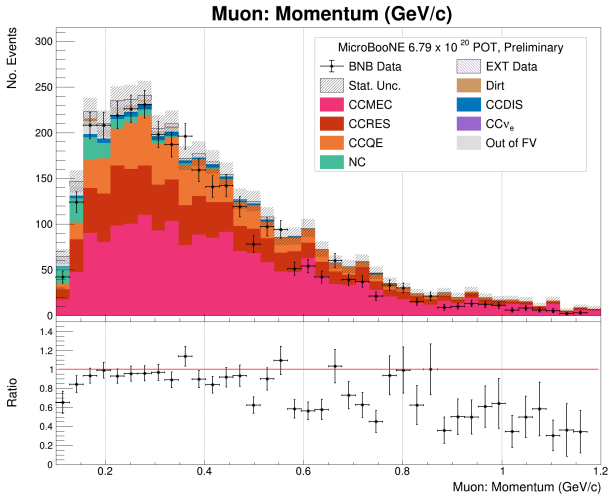

(b) Muon momentum: ν interactions.

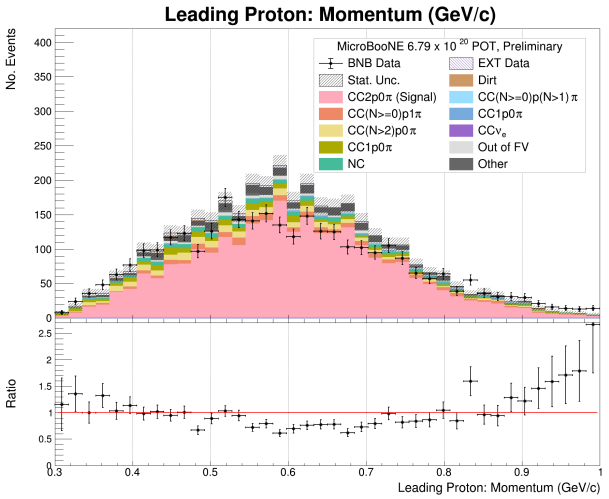

(c) Leading Proton momentum: ν topologies.

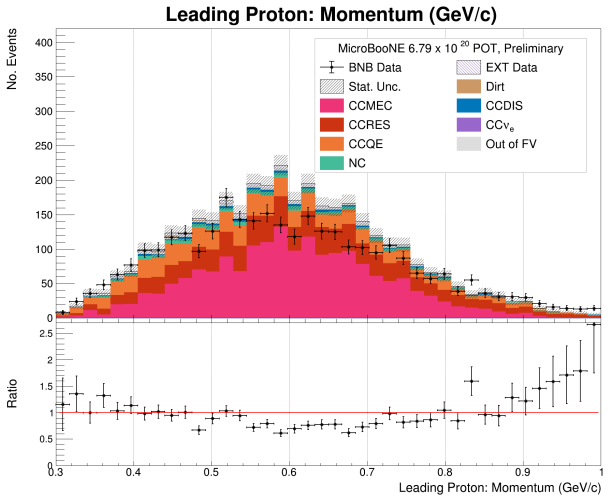

(d) Leading Proton momentum: ν interactions.

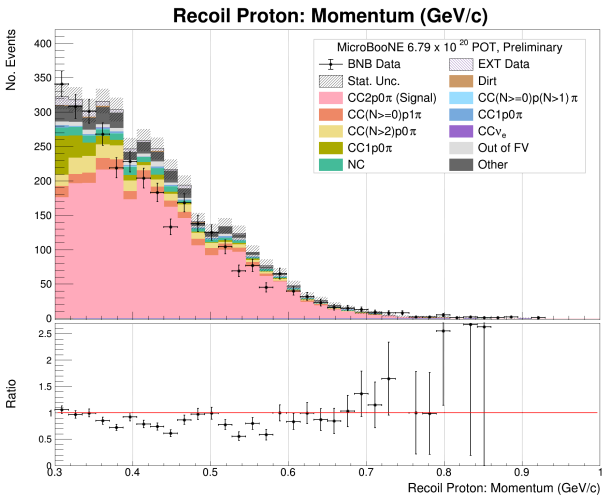

(e) Recoil Proton momentum: ν topologies.

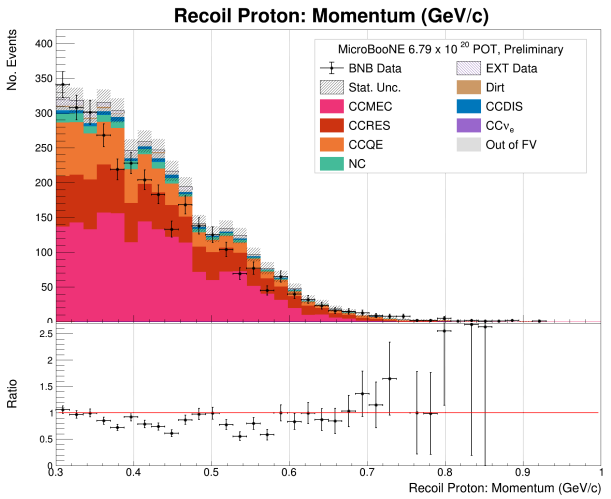

(f) Recoil Proton momentum: ν interactions.

Figure 10: Momentum of the three particles. Plots on the left show the MC-Overlay broken down into ν topologies. Plots on the right show the MC-Overlay broken down into ν channels.

The CC2p0π signal (pink band in plots on the left of Figure 10) and the CCMEC (magenta band in plots on the right of Figure 10), exhibit a shape which is similar to that of the selected data events (black). Even without full systematic uncertainties, we see relatively good data-MC agreement over the momentum range of all three particles.

From the momentum of the particles, we can calculate $\cos(\gamma_{\mathrm{Lab}})$ (Figure 11) and $\cos(\gamma_{\mu,\mathrm{p_{Lead}}+\mathrm{p_{Recoil}}})$ (Figure 12),which are the opening angle between the protons in the lab frame, and the opening angle between the muon momentum vector and the total proton momentum vector, respectively. These plots show events selected in the EXT-data, MC-Overlay, and MC-Dirt samples only. We have chosen to exclude BNB-data at this time until systematic uncertainties are fully evaluated. In the $\cos(\gamma_{\mathrm{Lab}})$ distribution, the CC2p0π signal (pink band in plots on the left of Figure 11) and the CCMEC (magenta band in plots on the right of Figure 11) both show a preference towards protons in the back-to-back configuration in the lab frame.

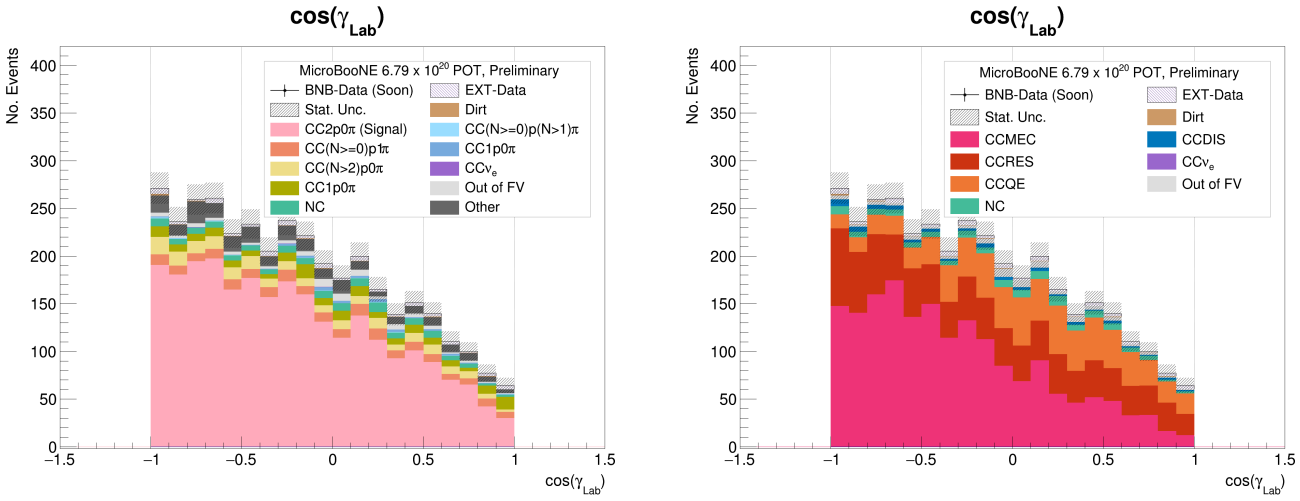

(a) $\cos(\gamma_{\mathrm{Lab}})$: ν topologies.

(b) $\cos(\gamma_{\mathrm{Lab}})$: ν interactions.

Figure 11: $\cos(\gamma_{\mathrm{Lab}})$. Plots on the left show the MC-Overlay broken down into ν topologies. Plots on the right show the MC-Overlay broken down into ν channels.

The $\cos(\gamma_{\mu,\mathrm{p_{Lead}}+\mathrm{p_{Recoil}}})$ dsitribution has a peak at -1 in both plots, primarily from true neutral current events (NC, teal band) and events where the true vertex lies outside of the defined FV (Out of FV, light grey band). Furthermore, the CC2p0π signal (pink band in plots on the left of Figure 11) and the CCMEC (magenta band in plots on the right of Figure 11) both show bumps in the distribution centered around a $\cos(\gamma_{\mu,\mathrm{p_{Lead}}+\mathrm{p_{Recoil}}})$ of 0.2-0.3.

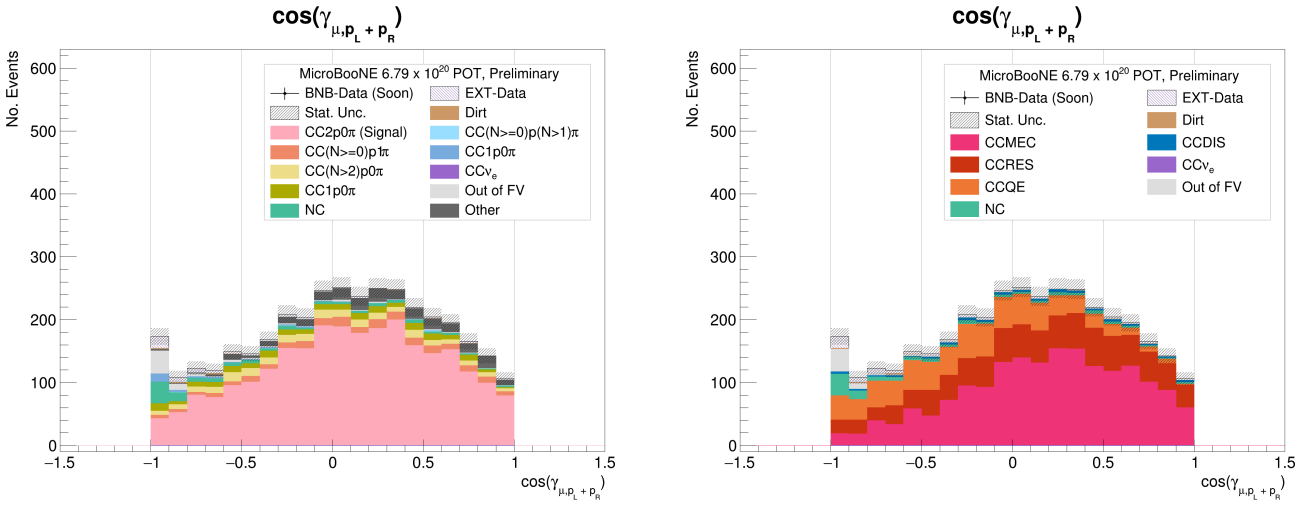

(a) $\cos(\gamma_{\mu,\mathrm{p_{Lead}}+\mathrm{p_{Recoil}}})$: ν topologies.

(b) $\cos(\gamma_{\mu,\mathrm{p_{Lead}}+\mathrm{p_{Recoil}}})$: ν interactions.

Figure 12: $\cos(\gamma_{\mu,\mathrm{p_{Lead}}+\mathrm{p_{Recoil}}})$. Plots on the left show the MC-Overlay broken down into ν topologies. Plots on the right show the MC-Overlay broken down into ν channels.

7 Conclusions and Future Work

In this note, we show progress in the investigation of 2p2h events in MicroBooNE. Studies of three different MEC theory models indicate that the momentum of the three different particles, the opening angle between the protons in the lab frame, and the opening angle between the muon momentum vector and the total proton momentum vector are sensitive to differences between the different MEC models. An event selection to identify CC2p0π events in data was developed, where the efficiency of the selection and the purity of the selected events, according to MC, were 13% and 65.4% respectively. Data-MC comparisons of the momentum of the three identified particles show relatively good agreement. Additionally, the event selection shows good coverage over all the variables of interest. Future work will involve the extraction of the CC2p0π differential cross-section and evaluation of systematic uncertainties. Results will be compared with predictions from the 3 different theoretical models presented in this note. Work is also in progress to create a model set in which contributions from SRCs are considered under the Generalized Contact Formalism (GCF) [17, 18]. Results will also be compared with events generated from this GCF model set. Corrections for detector resolution will be applied to make the data usable by the broader community.

A Appendices

A.1 Theoretical Studies Plots

A.1.1 cos(θ) and ϕ of the Three Particles

The following angles describe the direction of the track in the detector. The angle θ represents the angle of the track with respect the beam. The angle ϕ represents the direction of the track in the x-y plane. A diagram of these two angles can be found in Figure 13. Plots of cos(θ) are found in Figure 14 and plots of ϕ are found in Figure 15.

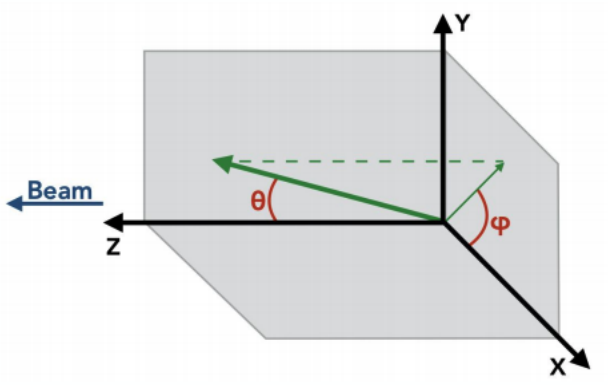

Figure 13: Diagram of θ and ϕ angles in the MicroBooNE detector

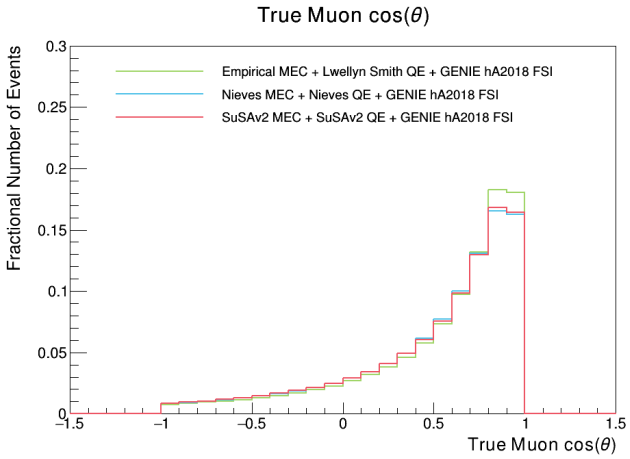

(a) Muon cos(θ).

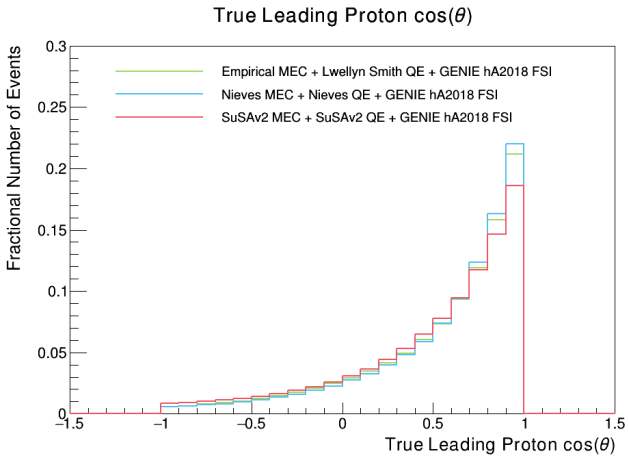

(b) Leading Proton cos(θ).

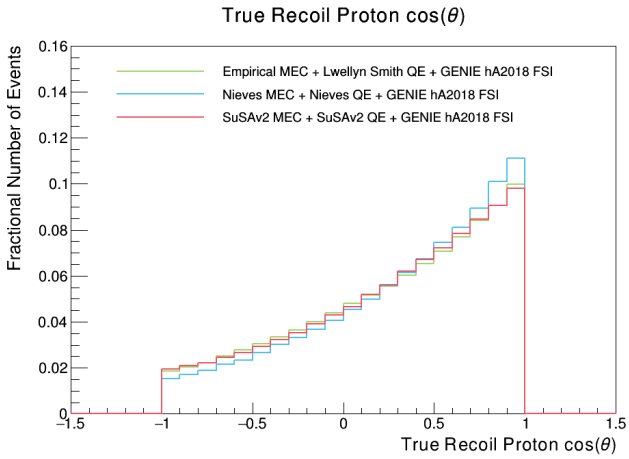

(c) Recoil Proton cos(θ).

Figure 14: cos(θ) of the three particles.

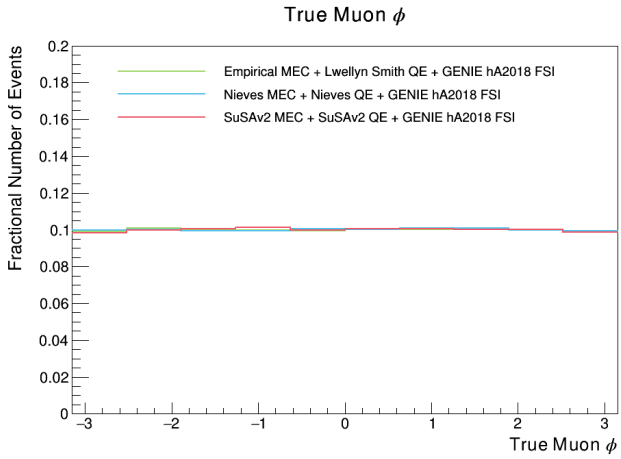

(a) Muon $\cos(\theta)$.

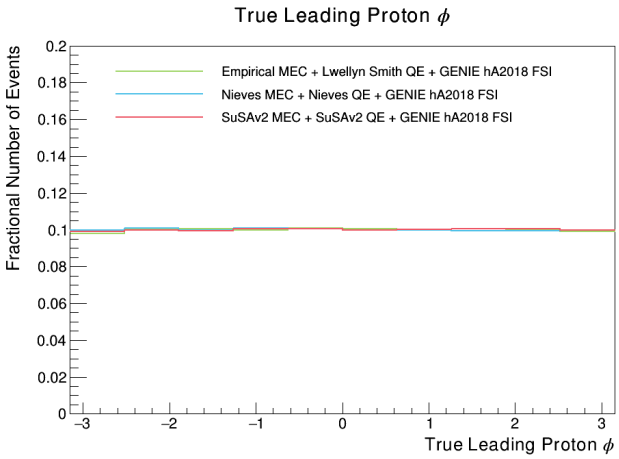

(b) Leading Proton $\cos(\theta)$.

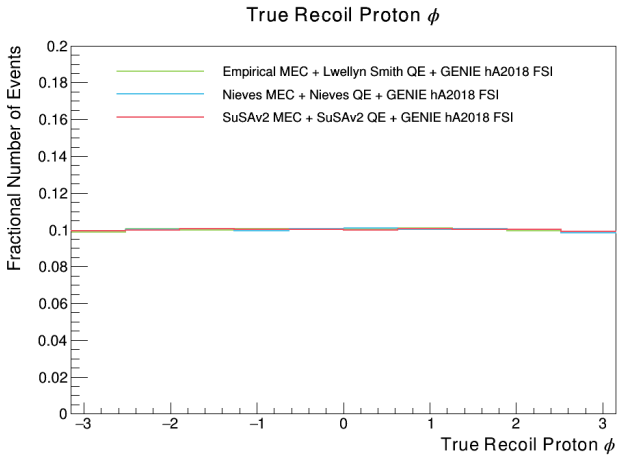

(c) Recoil Proton $\cos(\theta)$.

Figure 15: ϕ of the three particles.

A.1.2 Single Transverse Variables

We consider three variables known as the single transverse variables (STVs) in this section. These variables are of particular interest in this analysis since they are sensitive to a variety of nuclear effects such as Fermi motion, final state interactions, and multi-nucleon interactions (such as 2p2h). Three parameters, δp_T, $\delta\alpha_T$, and $\delta\phi_T$ are defined by projecting the lepton, $\vec{p}^{\,l}$, and the sum of the two proton momenta, ($\vec{p}^{\,p} = \vec{p}^{\,Lead} + \vec{p}^{\,Recoil}$, onto the transverse plane, as shown in Figure 16 [19]. The utilization of the sum of the proton momenta is different from existing measurements of STVs, which focus on using just the leading proton momentum.

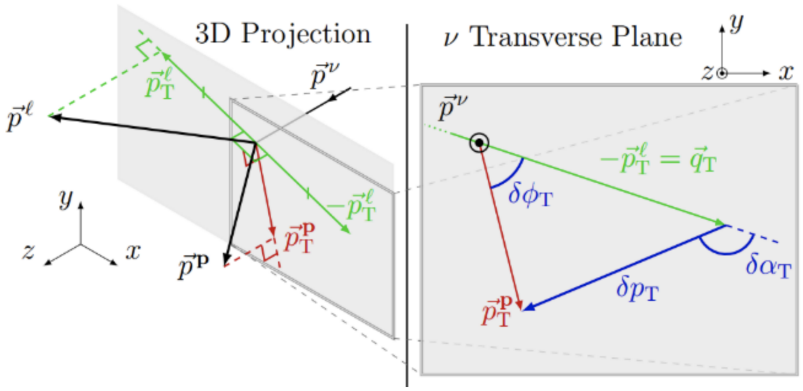

Figure 16: Diagram of the single transverse variables δp_T, $\delta\alpha_T$, and $\delta\phi_T$ [19].

The system can then be characterized by defining the vector magnitude of the total transverse momentum (Equation 3), the angle between the transverse lepton momentum and the total transverse proton momentum (Equation 4), and the angle between the transverse lepton and proton momentum (Equation 5) [20].

$$\delta p_T = |\vec{p_T}^{\,l} + \vec{p_T}^{\,p}| \tag{3}$$

$$\delta\alpha_T = \arccos\left(\frac{-\vec{p_T}^{\,l} \cdot \vec{\delta p_T}}{p_T^l \cdot \delta p_T}\right) \tag{4}$$

$$\delta\phi_T = \arccos\left(\frac{-\vec{p_T}^{\,l} \cdot \vec{p_T}^{\,p}}{p_T^l \cdot p_T^p}\right) \tag{5}$$

The transverse muon momentum and the total transverse proton momentum vectors will be equal and opposite if nuclear effects are absent, thereby causing δp_T and $\delta\phi_T$ to have peaks near 0. Any deviations from this special case are direct indicators of specific nuclear effects. If FSIs are present, $\delta\alpha_T$ will show directional preference. The STVs (with the leading proton and recoil proton momentum added together) for the selected events from the 3 different model sets can be found in Figure 17.

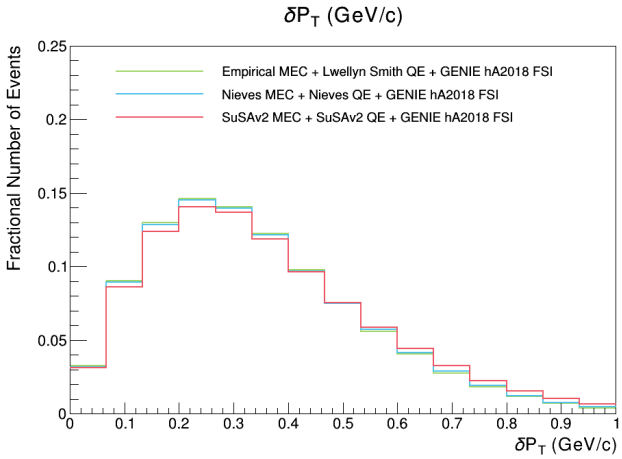

(a) δp_T

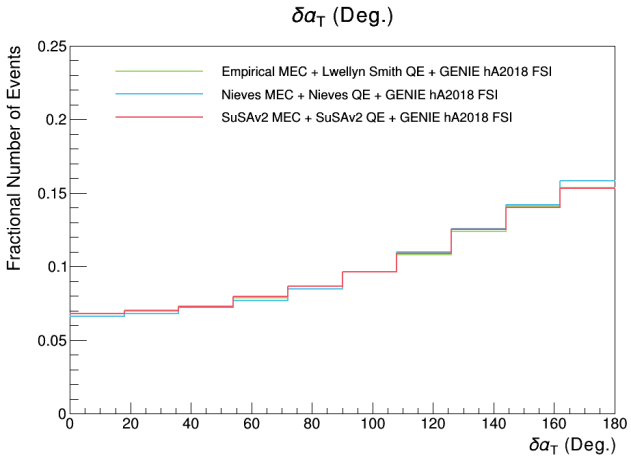

(b) $\delta\alpha_T$

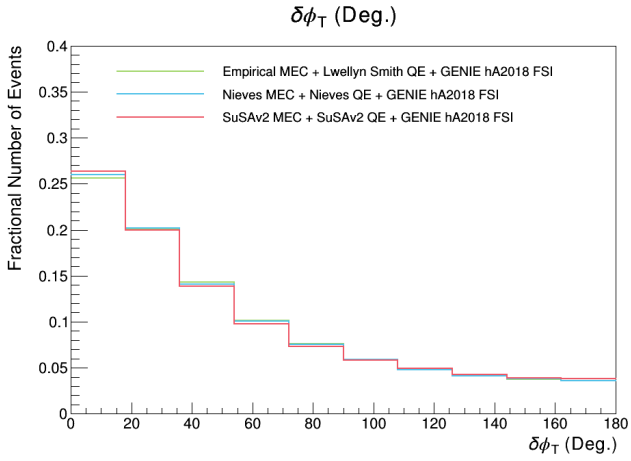

(c) $\delta\phi_T$

Figure 17: STVs with proton momentum added together.

A.1.3 True Initial Struck Nucleon Momentum

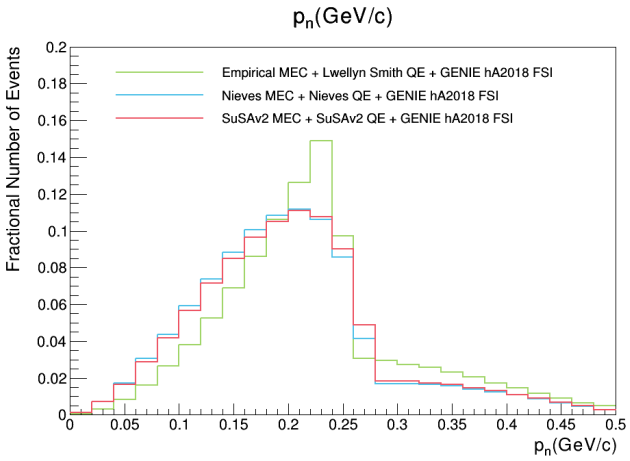

(a) p_n

Figure 18: True Initial Struck Nucleon Momentum.

A.1.4 True Neutrino Energy

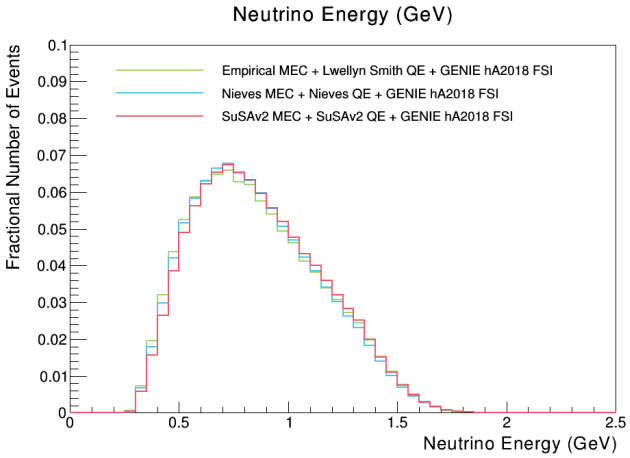

(a) True E_ν

Figure 19: True incident neutrino energy.

A.2 Selected EXT-Data, MC-Overlay, and MC-Dirt Distributions

A.2.1 cos(θ) of the Three Particles

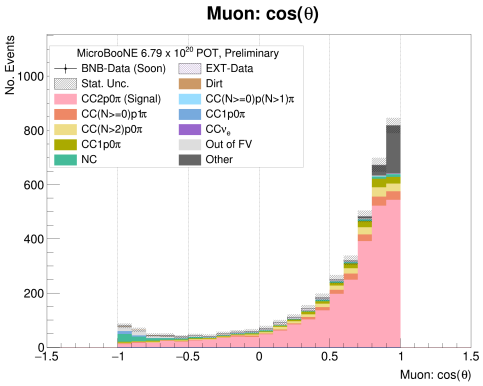

(a) Muon cos(θ): ν topologies.

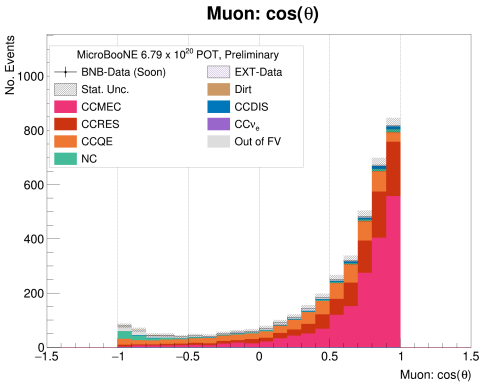

(b) Muon cos(θ): ν interactions.

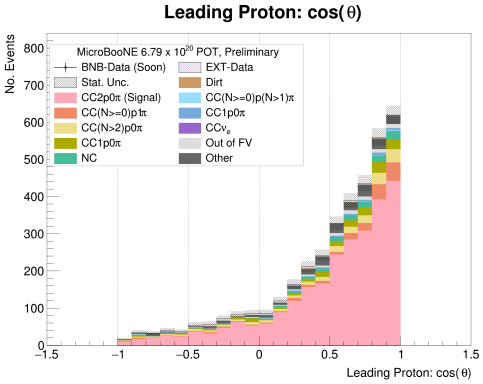

(c) Lead Proton cos(θ): ν topologies.

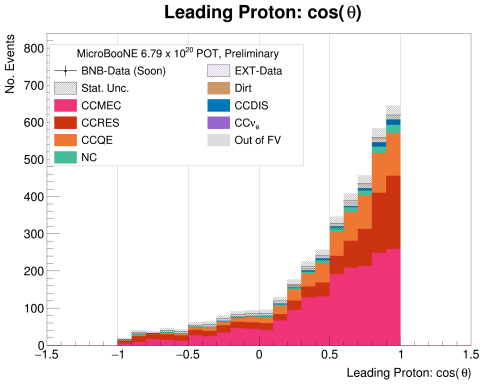

(d) Recoil Proton cos(θ): ν interactions.

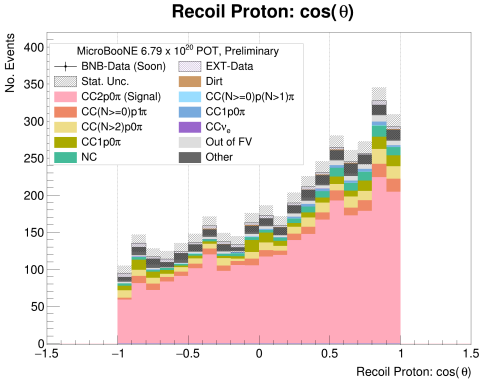

(e) Recoil Proton cos(θ): ν topologies.

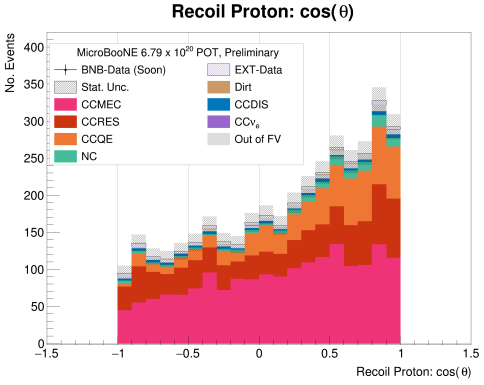

(f) Recoil Proton cos(θ): ν interactions.

Figure 20: cos(θ) of the three particles. Plots on the left show the MC-Overlay broken down into ν topologies. Plots on the right show the MC-Overlay broken down into ν channels.

A.2.2 ϕ of the Three Particles

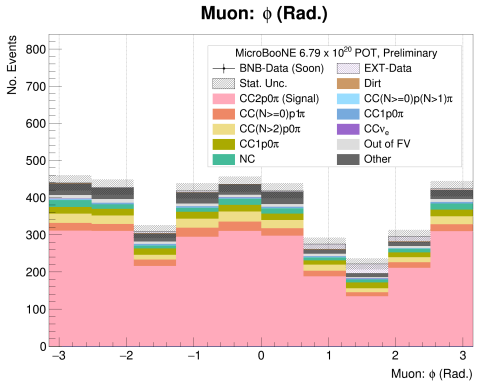

(a) Muon ϕ: ν topologies.

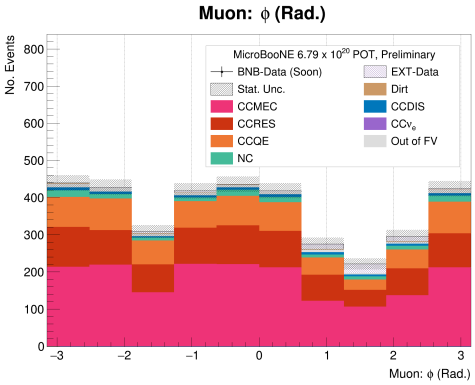

(b) Muon ϕ: ν interactions.

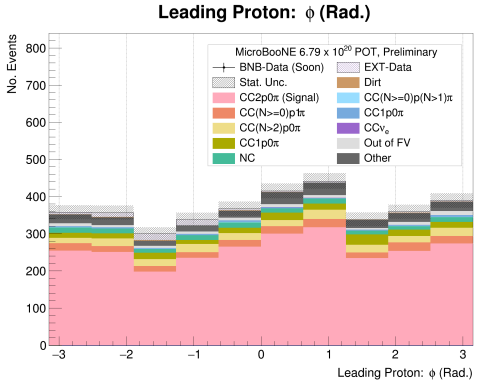

(c) Lead Proton ϕ: ν topologies.

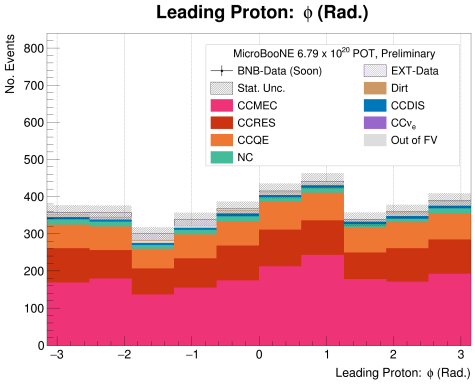

(d) Recoil Proton ϕ: ν interactions.

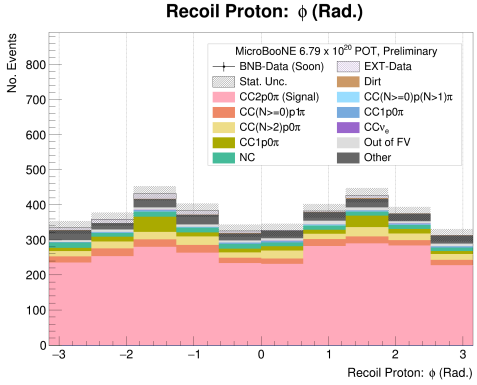

(e) Recoil Proton ϕ: ν topologies.

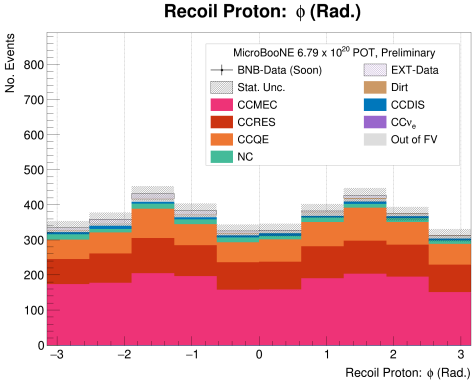

(f) Recoil Proton ϕ: ν interactions.

Figure 21: ϕ of the three particles. Plots on the left show the MC-Overlay broken down into ν topologies. Plots on the right show the MC-Overlay broken down into ν channels.

A.2.3 STVs

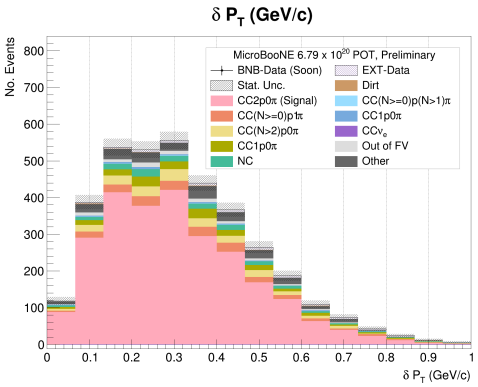

(a) δp_T: ν topologies.

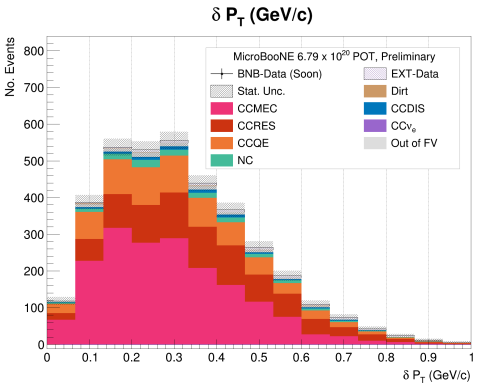

(b) δp_T: ν interactions.

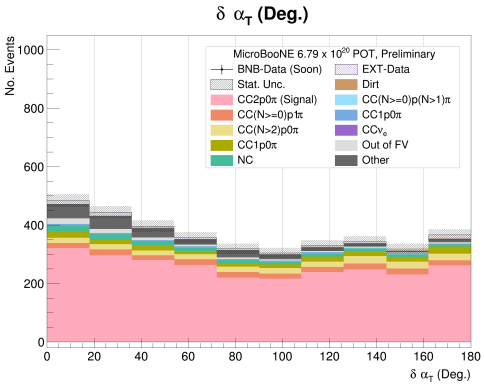

(c) $\delta\alpha_T$: ν topologies.

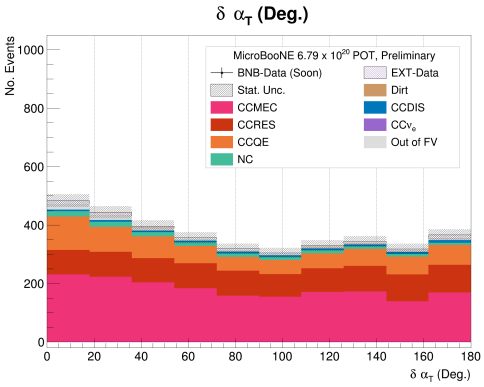

(d) $\delta\alpha_T$: ν interactions.

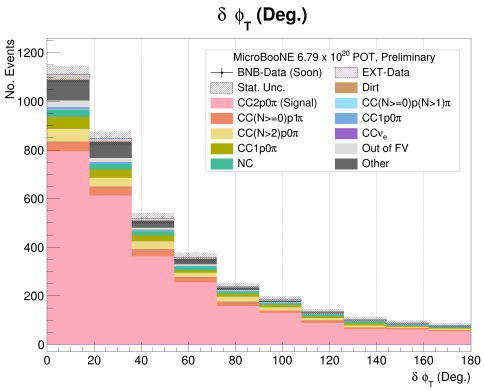

(e) $\delta\phi_T$: ν topologies.

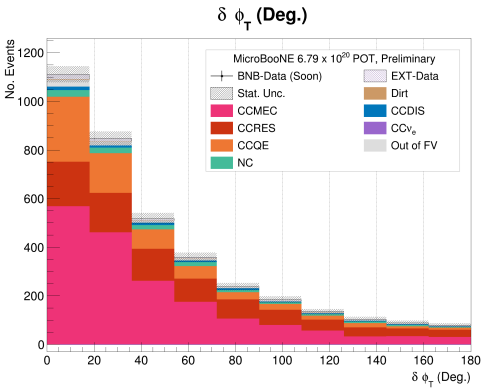

(f) $\delta\phi_T$: ν interactions.

Figure 22: STVs with proton momentum added together. Plots on the left show the MC-Overlay broken down into ν topologies. Plots on the right show the MC-Overlay broken down into ν channels.

A.2.4 Estimate of Initial Struck Nucleon Momentum

We can make an estimate for the initial-state nucleon momentum by utilizing the total transverse momentum from the STVs. The initial-state nucleon momentum can be estimated as

$$\mathrm{p_n} = \sqrt{\delta \mathrm{p_T^2} + \delta \mathrm{p_L^2}} \tag{6}$$

where $\delta \mathrm{p_T}$ is the total transverse momentum and $\delta \mathrm{p_L}$ is the total longitudinal momentum. The total longitudinal momentum is estimated as

$$\delta \mathrm{p_L} = \frac{1}{2} R - \frac{m_{A'}^2 + \mathrm{p_T^2}}{2\mathrm{R}} \tag{7}$$

$$R \equiv m_A + p_L^{\mu} + p_L^P - E^{\mu} - E^p \tag{8}$$

where $\mathrm{m}_{A^{(\prime)}}$ is the mass of the nuclear target (remnant) and $\mathrm{E}^{\mu(p)}$ is the muon (proton) energy. We take m_A to have a value of 37.21556 GeV/c^2 and $\mathrm{m}_{A'}$ to have a value of 37.21682 GeV/c^2. A plot of p_n can be seen in Figure 23.

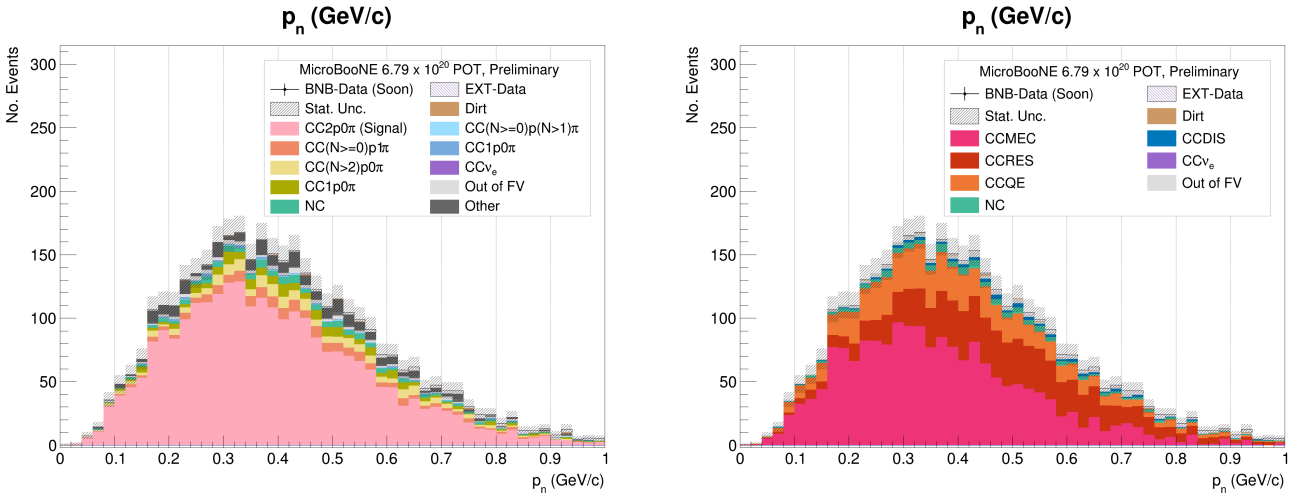

(a) p_n: ν topologies.

(b) p_n: ν interactions.

Figure 23: Estimate of the initial state neutron momentum. Plots on the left show the MC-Overlay broken down into ν topologies. Plots on the right show the MC-Overlay broken down into ν channels.

A.2.5 Estimate of Neutrino Energy

In addition to the initial struck nucleon momentum, we can also estimate the energy of the incident neutrino. Following [2], we calculated an estimate for the energy of the neutrino using the following Equation:

$$E_{\nu} = E_{\mu}^{tot} + E_{p1}^{KE} + E_{p2}^{KE} + T_{A-2} + E_{miss} \tag{9}$$

$$T_{A-2} = \frac{{P_{miss}^T}^2}{2 * M_{A-2}} \tag{10}$$

$$P_{miss}^T = |\vec{p}_{\mu}^{\,T} + \vec{p}_{p1}^{\,T} + \vec{p}_{p2}^{\,T}| \tag{11}$$

where E_{miss} is the missing energy (which contains both nucleon separation energy and the excitation level of the argon nucleus and we take this value to be 30.4 MeV), T_{A-2} is the kinetic energy of the A-2

system (where M_{A-2} is taken to be 35.37 MeV/c^2), and P^T_{miss} is the total transverse momentum of the system [2]. The plot of the neutrino energy using this estimate can be found in Figure 24. The peak of the distribution is lower than the estimated 0.7 GeV calculated from MicroBooNE neutrino flux estimates. This is expected as the selection preferentially selects muons with lower momentum.

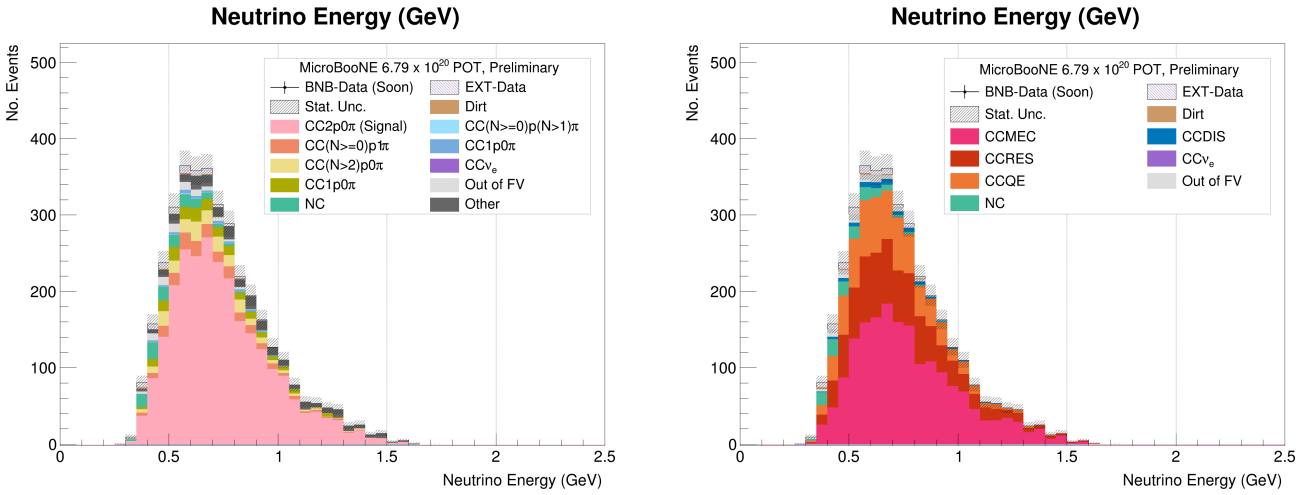

(a) E_ν: ν topologies.

(b) E_ν: ν interactions.

Figure 24: Estimate of the incident neutrino energy. Plots on the left show the MC-Overlay broken down into ν topologies. Plots on the right show the MC-Overlay broken down into ν channels.

References

[1] A. A. Aguilar-Arevalo et al. Significant Excess of ElectronLike Events in the MiniBooNE Short-Baseline Neutrino Experiment. *Phys. Rev. Lett.*, 121(22):221801, 2018.

[2] R. Acciarri et al. Detection of Back-to-Back Proton Pairs in Charged-Current Neutrino Interactions with the ArgoNeuT Detector in the NuMI Low Energy Beam Line. *Phys. Rev. D*, 90(1):012008, 2014.

[3] Teppei Katori. Meson Exchange Current (MEC) Models in Neutrino Interaction Generators. *AIP Conf. Proc.*, 1663(1):030001, 2015.

[4] Luis Alvarez-Ruso et al. Recent highlights from GENIE v3. 6 2021.

[5] J. Nieves, I. Ruiz Simo, and M. J. Vicente Vacas. Inclusive Charged–Current Neutrino–Nucleus Reactions. *Phys. Rev. C*, 83:045501, 2011.

[6] T. W. Donnelly and Ingo Sick. Superscaling in inclusive electron - nucleus scattering. *Phys. Rev. Lett.*, 82:3212–3215, 1999.

[7] R. Acciarri et al. Design and Construction of the MicroBooNE Detector. *JINST*, 12(02):P02017, 2017.

[8] Lauren E. Yates. MicroBooNE Investigation of Low-Energy Excess Using Deep Learning Algorithms. In *Meeting of the APS Division of Particles and Fields*, 10 2017.

[9] MicroBooNE Collaboration. New theory-driven genie tune for microboone. 2020.

[10] C. Adams et al. Ionization electron signal processing in single phase LArTPCs. Part I. Algorithm Description and quantitative evaluation with MicroBooNE simulation. *JINST*, 13(07):P07006, 2018.

[11] C. Adams et al. Ionization electron signal processing in single phase LArTPCs. Part II. Data/simulation comparison and performance in MicroBooNE. *JINST*, 13(07):P07007, 2018.

[12] R. Acciarri et al. The Pandora multi-algorithm approach to automated pattern recognition of cosmic-ray muon and neutrino events in the MicroBooNE detector. *Eur. Phys. J. C*, 78(1):82, 2018.

[13] MicroBooNE Collaboration. The pandora multi-algorithm approach to automated pattern recognition in lar tpc detectors. 2016.

[14] Wouter Van De Pontseele. *Search for Electron Neutrino Anomalies with the MicroBooNE Detector*. PhD thesis, Oxford U., 2020.

[15] P. Abratenko et al. Calorimetric classification of track-like signatures in liquid argon tpcs using microboone data. 8 2021.

[16] MicroBooNE Collaboration. Double-differential measurements of mesonless charged-current muon neutrino interactions on argon with final-staate protons using the microboone detector. 2021.

[17] Ronen Weiss, Igor Korover, Eli Piasetzky, Or Hen, and Nir Barnea. Energy and momentum dependence of nuclear short-range correlations - spectral function, exclusive scattering experiments and the contact formalism. *Physics Letters B*, 791, 02 2019.

[18] R. Weiss, R. Cruz-Torres, N. Barnea, E. Piasetzky, and O. Hen. The nuclear contacts and short range correlations in nuclei. *Phys. Lett. B*, 780:211–215, 2018.

[19] Stephen Dolan. Probing Nuclear Effects at the T2K Near Detector Using Transverse Kinematic Imbalance. In *Prospects in Neutrino Physics*, 4 2016.

[20] K. Abe et al. First t2k measurement of transverse kinematic imbalance in the muon-neutrino charged-current single-π^+ production channel containing at least one proton. *Phys. Rev. D*, 103:112009, Jun 2021.

List of Figures

List of Tables